

Simulation of granular jet: Is granular flow really a “perfect fluid?”

Tomohiko Sano and Hisao Hayakawa

Yukawa Institute for Theoretical Physics, Kyoto University Kitashirakawa Oiwakecho, Sakyo-ku, Kyoto 606-8502 Japan

We perform a three-dimensional simulation of granular jet for both frictional and frictionless grains. Through our simulation we confirm that the system after an impact of the jet has a finite viscosity for both frictional and frictionless grains. This result is contrast to the suggestion in an experiment of granular jet [X. Cheng *et al.*, Phys. Rev. Lett. **99**, 188001 (2007)], in which there exists an analogy between granular jets and quark-gluon plasma.

PACS numbers: 45.70.Mg, 83.10.Rs, 05.20.Dd

Introduction: The impact processes play important roles in various fields such as nuclear reactions[1–3], atomic collisions[4, 5], hydrodynamics[6–9] and granular physics[10–16]. Recent experimental and numerical studies revealed interesting aspects of impact processes of a granular flow. At low volume fractions, impact of a granular flow onto a wall produces a shock, which quantitatively agrees with the Mach cone produced by supersonic gas flow[11–13]. The impact dynamics of granular particles is important not only for industrial applications, e.g. ink-jet printing and blast cleaning[17, 18], but also for geophysical problems such as the formation of craters[14–16].

Recently, an experimental paper on dense granular jets[10] has reported that fluid state after the impact is similar to that for quark-gluon plasma (QGP) achieved in heavy ion hadron colliders, where QGP behaves as a fluid with very small viscosity[1–3]. Quite recently, Elowitz *et al.*[19] demonstrated that the solution of inviscid Euler equation is almost identical to that obtained from a molecular dynamics simulation for inelastic hard core particles, at least, for two dimensional frictionless grains. These results are counter intuitive because the dense granular fluid has a large viscosity in usual setup[20].

The purpose of this Letter is to clarify whether the granular fluid after the jet impact on a fixed wall actually behaves as a perfect fluid. So far all numerical studies[19, 21, 22] are two-dimensional ones for this problem, we perform a three dimensional molecular dynamics simulation for soft core particles to compare our results with experimental results.

Model: We adopt the discrete element method (DEM) for mono-disperse soft core particles of the diameter d [23, 24]. The reason why we adopt a soft core model is the following. The DEM can be used even for dense systems above the jamming point, while the simulation in terms of the event driven algorithm cannot be free from inelastic collapse[25] and cannot reach the jamming point. DEM has also an advantage when we consider the effect of friction and rotation of grains. Indeed, the event-driven algorithm for frictional grains is complicated, but DEM for frictional grains is simple. When the particle i at the position \mathbf{r}_i and the particle j at \mathbf{r}_j are in contact, the normal force F_{ij}^n is described as $F_{ij}^n \equiv F_{ij}^{(el)} + F_{ij}^{(vis)}$ with $F_{ij}^{(el)} \equiv k_n(d - r_{ij})$ and $F_{ij}^{(vis)} \equiv -\eta_n(\mathbf{g}_{ij} \cdot \hat{\mathbf{r}}_{ij})$, where

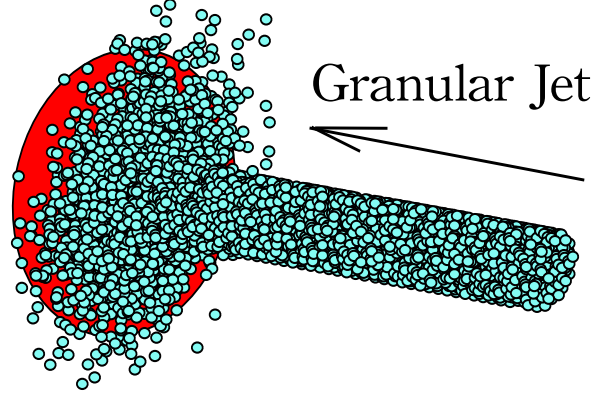


FIG. 1: (Color online) Snapshot of a three-dimensional simulation.

$r_{ij} \equiv |\mathbf{r}_i - \mathbf{r}_j|$ and $\mathbf{g}_{ij} \equiv \mathbf{v}_i - \mathbf{v}_j$ with the velocity \mathbf{v}_i of the particle i . The tangential contact force is given by $F_{ij}^t \equiv \min\{|\tilde{F}_{ij}^t|, \mu F_{ij}^n\} \text{sign}(\tilde{F}_{ij}^t)$, where μ is the friction constant, $\text{sign}(x) = 1$ for $x \geq 0$ and $\text{sign}(x) = -1$ for otherwise, $\tilde{F}_{ij}^t \equiv k_t \delta_{ij}^t - \eta_t \dot{\delta}_{ij}^t$ with the tangential overlap δ_{ij}^t between i and j particles and the tangential component of relative velocity $\dot{\delta}_{ij}^t$ between i th and j th particles. Here, we adopt parameters $k_t = 0.2k_n$, $\eta_t = 0.5\eta_n$, $\mu = 0.2$, $k_n = 4.98 \times 10^2 m u_0^2 / d^2$ and $\eta_n = 2.88 u_0 / d$, where u_0 is the incident velocity and m is the particle mass. Experimentally, it is known that the friction constant of spheres is $\mu = 0.175 \pm 0.1$ [26]. This set of parameters implies that the restitution coefficient for normal impact is $e = 0.75$ and duration time is $t_c = 0.10d/u_0$. We adopt the second-order Adams-Bashforth method for the time integration with the time interval $\Delta t = 0.02t_c$ through our simulation. We fix the jet diameter $D_{\text{jet}}/d = 10.0$ and the target diameter $D_{\text{tar}}/d = 22.0$. We generate an initial configuration as follows. We prepare fcc crystals and remove particles randomly to reach the desired density. The initial granular temperature, which represents the fluctuation of particles motion, is zero. We control the initial volume fraction $\phi_0/\phi_{\text{fcc}} \equiv \tilde{\phi}_0$ before the impact as $0.30 \leq \tilde{\phi}_0 \leq 0.90$ with volume fraction for a fcc crystal $\phi_{\text{fcc}} \simeq 0.74$. We use 20,000 particles for our simulations. The wall consists of one-layer particles, which are connected each other and with their own initial po-

sitions via the spring and the dashpot. Here, the spring constant and the dashpot constant for the wall particles are given by $k_p = 10.0mu_0^2/d^2$ and $\eta_p = 5.0\eta_n$, respectively. It is known that the collective motion of particles near the wall is almost frozen[19], while the granular temperature near the wall is higher than that in the other regions.

Figure 1 is a snapshot of our simulation on the impact of granular jet. The scattering angle exhibits the crossover cone-like structure to sheet-like one, depending on $D_{\text{tar}}/D_{\text{jet}}$, which is almost independent of the restitution coefficient[27].

We evaluate physical quantities near the wall whose height is $z = \Delta z \equiv 5.0d$ from the wall $z = 0$ in our simulations. We divide the cylindrical calculation region into the radial direction $r = 0, \Delta r, 2\Delta r, \dots, 5\Delta r$, with $\Delta r \equiv R_{\text{tar}}/5$ and the target radius R_{tar} . Physical quantities are estimated in k th mesh region with $k\Delta r < r < (k+1)\Delta r$ ($k = 0, 1, \dots, 5$) and $0 < z < \Delta z$.

Stress tensor: Let us evaluate the stress tensor near the wall as in Ref. [28]. The stress tensor $\sigma_{\alpha\beta}(\mathbf{r})$ at \mathbf{r} consists of the kinetic part $\sigma_{\alpha\beta}^k(\mathbf{r})$ and the contact stress $\sigma_{\alpha\beta}^c(\mathbf{r})$ as

$$\sigma_{\alpha\beta}(\mathbf{r}) = \sigma_{\alpha\beta}^k(\mathbf{r}) + \sigma_{\alpha\beta}^c(\mathbf{r}), \quad (1)$$

where their microscopic definitions are respectively given by

$$\sigma_{\alpha\beta}^k(\mathbf{r}) = \frac{1}{V} \sum_i m u_{i\alpha} u_{i\beta}, \quad (2)$$

$$\sigma_{\alpha\beta}^c(\mathbf{r}) = \frac{1}{V} \sum_{i < j} F_{\alpha}^{ij} r_{\beta}^{ij}, \quad (3)$$

where i and j are indices of particles, $\alpha, \beta = r, \theta, z$ denotes cylindrical coordinates and \sum denotes the summation over the particles located at \mathbf{r} . Here, z axis is parallel to the incident jet axis, and V is the volume of each mesh at \mathbf{r} and $u_{i\alpha} = v_{\alpha}^i - \bar{v}_{\alpha}$ with the mean velocity \bar{v}_{α} . To calculate the stress tensor in the cylindrical coordinates, we firstly calculate $\sigma_{\alpha'\beta'}$ in the Cartesian coordinate, $\alpha', \beta' = x, y, z$, whose original point is the same as the cylindrical one, and transform it into that for the cylindrical one.

Here we show the profile of the stress tensor for the frictional case (Fig. 2 for $\phi_0 = 0.90$). We average the data over ten different initial configurations. From Fig. 2, it is apparent that off-diagonal components of the stress tensor σ_{rz} and σ_{zr} are much smaller than diagonal components, where the ratio of the off-diagonal to the diagonal element is estimated as $|\sigma_{rz}/\sigma_{zz}| \simeq 1.7 \times 10^{-2}$ at $r/R_{\text{tar}} = 0.1$. This result supports that the solution of Euler equation well reproduce the granular flow after the impact [19]. We also found that there exists a large normal stress difference, which cannot be observed even for our two dimensional case. We obtain the ratio $|\sigma_{rz}/\sigma_{zz}| \simeq 3.0 \times 10^{-2}$ at $r/R_{\text{tar}} = 0.1$ for the frictionless case, where off-diagonal components are much smaller than diagonal ones as in the case of the frictional case.

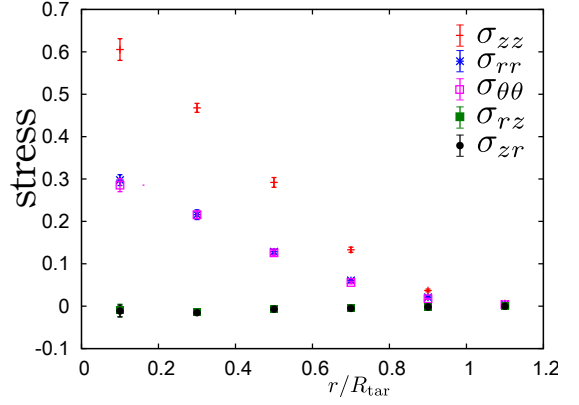


FIG. 2: (Color online) The profile of the stress tensor as the functions of distance from the jet axis r with R_{tar} for frictional grains with $\phi_0 = 0.90$. The off-diagonal components of the stress tensor σ_{rz} and σ_{zr} are much smaller than diagonal components as $|\sigma_{rz}/\sigma_{zz}| \simeq 1.7 \times 10^{-2}$ at $r/R_{\text{tar}} = 0.1$.

Pressure: Let us look at the result of the pressure here (Fig. 3). It is known that the granular sheared flow such as a chute flow and a plane shear flow can be approximately described by granular hydrodynamics with transport coefficient derived from the kinetic theory, i.e. the Enskog equation [29–34]. We adopt the transport coefficients derived by Garzó and Dufty[30] with the pressure $P \equiv \sum_{\alpha} \sigma_{\alpha\alpha}/3$, the density n , the volume fraction ϕ , and the granular temperature $T_g(\mathbf{r}) \equiv \sum_{i\alpha} m u_{i\alpha}^2/3N$. The pressure is conventionally given by

$$\frac{P}{nT_g} = 1 + 2\phi(1+e)\chi, \quad (4)$$

$$\chi = \begin{cases} \frac{1-\phi/2}{(1-\phi)^3} & (0 < \phi < \phi_f) \\ \frac{(1-\phi_f/2)(\phi_c-\phi_f)}{(1-\phi_f)^3(\phi_c-\phi)} & (\phi_f < \phi < \phi_c), \end{cases} \quad (5)$$

where $\phi_f = 0.49$ and $\phi_c = 0.64$ [35]. For the frictional case, in general, five equations for rotational degree of freedom are necessary, in addition to those for translational one. However, it is known that ten equations for frictional grains can be reduced to five equations by introducing effective coefficient of restitution \bar{e} if the friction constant μ is small [32–34]. According to this simplification we use the effective restitution coefficient $\bar{e} = 0.616$ for $e = 0.75$ and $\mu = 0.2$, for frictional case in the following.

Let us compare the theoretical curve with numerical results for several ϕ_0 (Fig. 3). The black solid line in Fig. 3 and that in the inset denote the theoretical curve for the frictionless case and the frictional case, respectively. Surprisingly, the expression for the pressure in Eq. (4) considerably reproduces the numerical result for $\phi < 0.5$ inspite of the existence of the normal stress difference, while Eq.(4) for $0.5 < \phi < 0.6$ may have significant deviation from the theoretical line. The deviation, which may result from the singularity at the source point around $r \simeq 0$, emerges only at $r/R_{\text{tar}} = 0.1$.

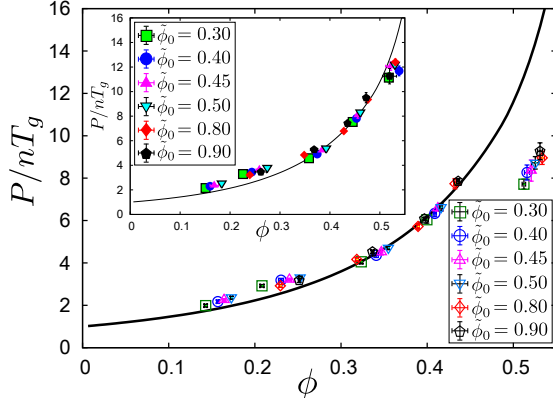


FIG. 3: (Color online) The comparison between the theoretical pressure in Eq. (4) and the observed pressure for several $\tilde{\phi}_0$, where the vertical axis is P divided by the density n and the granular temperature T_g for the frictionless case. The inset denotes comparison between those for the frictional case. Black solid lines in each figure denote Eq. (4) for the frictionless and the frictional case, respectively.

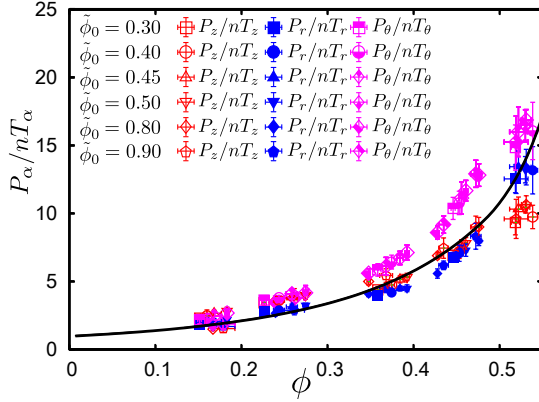


FIG. 4: (Color online) The diagonal components of the stress tensor for the frictional case with several $\tilde{\phi}_0$ divided by nT_α , where T_α is the temperature for α direction $T_\alpha \equiv \sum_i m u_{i\alpha}^2 / N$. Red empty points, blue filled points, purple half-filled points and the solid black line denote P_z/nT_z , P_r/nT_r , P_θ/nT_θ and Eq. (4), respectively.

Although there exists large normal stress differences, numerical results can be reproduced from the kinetic theory if we introduce the anisotropic temperature. Indeed, equations of state for each coordinates satisfies, $P_\alpha = nT_\alpha \{1 + 2\phi(1+e)\chi\}$ for $\alpha = r, \theta, z$ and $P_r = \sigma_{rr}$, $P_\theta = \sigma_{\theta\theta}$ and $P_z = \sigma_{zz}$. By summing up $P_\alpha = nT_\alpha \{1 + 2\phi(1+e)\chi\}$ over α , we obtain Eq. (4). From Fig. 4, we verify that P_z/nT_z and P_r/nT_r are on the theoretical curve for isotropic systems, but P_θ/nT_θ has a systematically larger value from the isotropic one. Although our suggestion that the anisotropy only appears through the normal stress is not perfect, the result gives a reasonable physical picture, at least, for r and z directions.

Shear viscosity: Let us evaluate the shear viscosity from the data of the stress tensor. The theoretical shear

viscosity for frictionless granular fluids, which depends on temperature and volume fraction, is given by

$$\sigma_{rz} = -\eta_{\text{kin}} D_{rz}, \quad (6)$$

$$\eta_{\text{kin}}(\phi, T_g) = \frac{5}{16d^2} \sqrt{\frac{mT_g}{\pi}} \eta^*(\phi) \quad (7)$$

with strain rate $D_{rz} \equiv (\partial \bar{v}_r / \partial z + \partial \bar{v}_z / \partial r) / 2$, $\eta^*(\phi) \equiv \eta^{k*} [1 + 4\phi\chi(1+e)/5] + 3\gamma^*/5$, $\eta^{k*} \equiv [1 - 2(1+e)(1-3e)\phi\chi/5] / (\nu_\eta^* - \zeta^*/2)$, $\gamma^* \equiv 128\phi^2\chi(1+e)(1-c^*/32)/5\pi$, $\nu_\eta^* = \chi[1 - (1-e)^2/4][1 - c^*/64]$, $\zeta^* \equiv 5\chi(1-e^2)(1+3c^*/32)/12$ and $c^* \equiv 32(1-e)(1-2e^2)/[81-17e+30e^2(1-e)]$ [30].

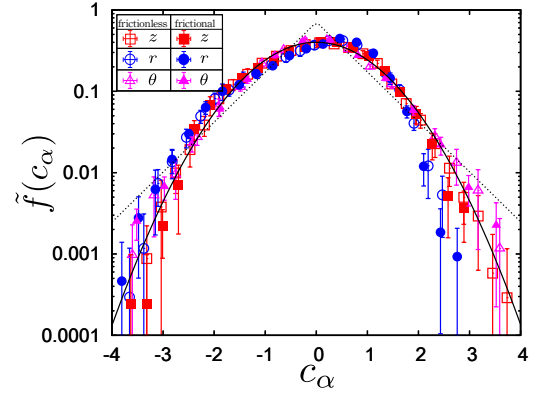


FIG. 5: (Color online) Scaled VDF $\tilde{f}(c_\alpha)$ for $\tilde{\phi}_0 = 0.90$. Empty points and filled points denote the frictionless case and the frictional case, respectively. The black solid line is $\tilde{f}(c_\alpha) = \exp(-c_\alpha^2/2)/\sqrt{2\pi}$ and the dashed line is $\tilde{f}(c_\alpha) = \exp(-\sqrt{2}|c_\alpha|)/\sqrt{2}$.

For the frictional case, yield stress σ_Y , which is the residual stress without deformation may exist in general. Thus, the constitutive equation in Eq. (6) is replaced by $\sigma_{rz} = \sigma_Y - \eta D_{rz}$, for this case. However, in this letter, we assume $\sigma_Y = 0$. The reason for the absence of the yield stress is based on the following three observations. The first reason is the velocity distribution functions (VDF), which is characterized by flatness of them. The VDF are near to the Gaussian for frictionless cases. On the other hand, the VDF for frictional cases are exponential-like[36]. We scale VDF $f(v_\alpha)$ as $\tilde{f}(c_\alpha) = v_{\alpha 0}^{-1} f(v_\alpha)$ with $\int dc_\alpha \tilde{f}(c_\alpha) = \int dc_\alpha c_\alpha^2 \tilde{f}(c_\alpha) = 1$, $\int dc_\alpha c_\alpha \tilde{f}(c_\alpha) = 0$ and $v_{\alpha 0} \equiv \sqrt{2T_\alpha/m}$ for each α . Scaled VDF for each velocity components are shown in Fig. 5, where all of the VDF are near to Gaussian $\tilde{f}(c_\alpha) = \exp(-c_\alpha^2/2)/\sqrt{2\pi}$ even for the frictional case, because friction constant $\mu = 0.2$ may be small, and are far from exponential-like VDF $\tilde{f}(c_\alpha) = \exp(-\sqrt{2}|c_\alpha|)/\sqrt{2}$. The flatness, which is defined as $\langle x^4 \rangle / \langle x^2 \rangle^2 = \langle x^4 \rangle$ for $\langle x^2 \rangle = 1$ with $\langle \dots \rangle \equiv \int dx \tilde{f}(x) \dots$, is summarized in TABLE I for $\tilde{\phi}_0 = 0.90$. It should be noted that the flatness with Gaussian VDF is 3.0 and that with exponential

TABLE I: Flatness for the frictionless and the frictional case.

	z	r	θ
frictionless case	2.87	2.86	3.41
frictional case	2.70	2.98	3.71

TABLE II: Extrapolated yield stress $-\sigma_Y \times 10^3$.

r/R_{tar} ϕ_0	0.30	0.50	0.70	0.90
0.30	6.41 ± 3.3	0.701 ± 1.5	0.434 ± 0.66	0.447 ± 0.26
0.40	7.54 ± 5.8	-0.159 ± 3.2	0.538 ± 1.1	0.364 ± 0.52
0.45	8.79 ± 2.3	0.800 ± 2.1	0.440 ± 0.94	0.783 ± 0.44
0.50	6.79 ± 2.8	-0.574 ± 1.9	0.632 ± 0.94	0.608 ± 0.32
0.80	7.00 ± 4.8	2.19 ± 1.7	-0.953 ± 1.3	0.392 ± 0.50
0.90	5.21 ± 2.7	-0.540 ± 2.9	-0.396 ± 1.2	0.243 ± 0.83

VDF is 6.0. Although the flatness with VDF for θ deviates slightly from 3.0, it is still far from 6.0, and thus, the effect of Coulombic slip with friction constant $\mu = 0.2$ is not significant. The second reason is the small Coulombic constant. In this case, renormalization of restitution coefficient is known to be valid[32–34]. We stress here that the residual stress for the frictional granular fluid with small Coulombic constant does not exist in the usual setup[37, 38] even for the jamming transition. Moreover, once we assume that shear viscosity corresponds to the value from the kinetic theory $\eta(r) = \eta_{\text{kin}}(\phi, T_g)$, the extrapolated σ_Y are obtained at each mesh, through $\sigma_{rz}(r) = \sigma_Y(r) - \eta_{\text{kin}}(\phi(r), T_g(r))D_{rz}(r)$. As a result, $\sigma_Y \simeq 0$ holds for $r/R_{\text{tar}} > 0.40$ (TABLE II). Thus, $\sigma_Y = 0$ is a self consistent assumption if we adopt the kinetic theory. For these reasons, we assume $\sigma_Y = 0$.

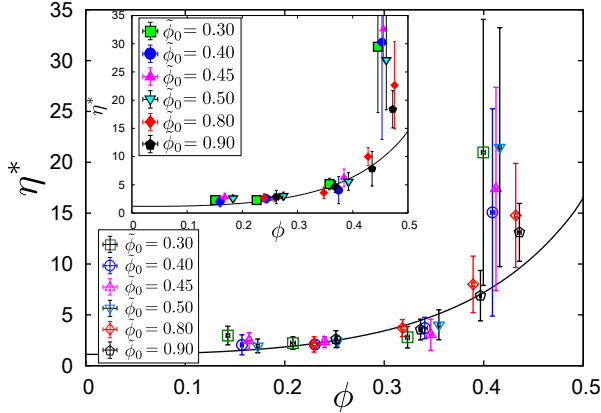


FIG. 6: (Color online) Non-dimensional shear viscosity η^* , which is defined in Eq. (7), for several ϕ_0/ϕ_{fcc} in $0.2R_{\text{tar}} < r < R_{\text{tar}}$. Black solid lines denote theoretical curves.

Now, let us try to compare the theoretical expression in Eq. (7) with the numerical measured shear viscosity. We estimate strain rate as $\partial \bar{v}_r(r, \Delta z/2)/\partial z \simeq (\bar{v}_r(r, 3\Delta z/4) - \bar{v}_r(r, \Delta z/4))/(\Delta z/2)$ and $\partial \bar{v}_z(r, z)/\partial r \simeq (\bar{v}_z(r + \Delta r/2, z) - \bar{v}_z(r - \Delta r/2, z))/\Delta r$. Since we evaluate the physical quantities near the wall, the mesh $0 < z <$

Δz is divided into $0 < z < \Delta z/2$ and $\Delta z/2 < z < \Delta z$ to calculate $\partial \bar{v}_r(r, \Delta z/2)/\partial z$ and $0 < r < R_{\text{tar}}$ is divided into $0 < r < \Delta r/2$, $\Delta r/2 < r < 3\Delta r/2, \dots$. The comparison of η^* , which is the non-dimensional shear viscosity in Eq. (7), for $0.2 < r/R_{\text{tar}} < 1.0$ is shown in Fig. 6. Although there is a slight deviation between them for large ϕ i.e. small r , which may be the effect of the singularity in the center $r = 0$, the theoretical curve reproduces other numerical results. We can, thus, conclude that the flow has the finite shear viscosity which has the same order of the predicted value by the kinetic theory. The reason why the simulations are approximately described by the Euler equation is that the strain rate itself is small i.e. $D_{rz}d/u_0 < 4.5 \times 10^{-2}$, and thus σ_{rz}/σ_{zz} is small.

Discussion: There exists large normal stress differences, which may not be considered in the kinetic theory. We found that the normal stress vertical to the wall is almost twice as large as the other diagonal components of the stress tensor. A unidirectional flow can be distributed into two directions in the usual time revolution. This mechanism might be easily understood by the time reversal flow in which two directional flow merge into a unidirectional flow. This picture is possible to be considered because the dissipation is not crucially important, at least, for the scattering angle[27]. Thus, the fluctuations in r and θ components may be half of that in z component. Therefore, we may understand the relation $T_z \simeq 2T_\theta \simeq 2T_r$.

Conclusion: We have numerically investigated the granular jet which impacts on a fixed wall. We revealed that the granular flow after the impact has the finite shear viscosity which has the same order of the predicted value by the kinetic theory, and thus the similarity between the granular flow and the perfect fluid is superficial, which comes from a small strain rate. This result is consistent with the result of the experiment[10] and is contrast to the two dimensional simulations for an inviscid fluid[19, 21]. We have assumed $\sigma_Y = 0$, judging from VDF, small Coulombic constant and extrapolated σ_Y . This assumption is strong one for the comparison between the kinetic theory and the our data, but the validity of this assumption for larger Coulombic constant will be discussed later. Although both the pressure and the viscosity are not far from the predictions by the kinetic theory, there exists a large normal stress difference in contrast to the case of the kinetic theory. Our results may shed the light on the internal fluid structure under a strong nonequilibrium situation, i.e. the impact processes of the granular jet.

Acknowledgments

We would like to thank W. W. Zhang and T. Hirano for fruitful discussions. This work is partially supported by and the Grant-in-Aid for the Global COE program “The Next Generation of Physics, Spun from Universality and Emergence from MEXT, Japan.

-
- [1] K. H. Ackermann *et al.* (STAR Collaboration), Phys. Rev. Lett. **86** 402 (2001).
 - [2] P. K. Kovtun, D. T. Son, and A. O. Starinets, Phys. Rev. Lett. **94** 111601 (2005).
 - [3] T. Hirano, and Y. Nara, Phys. Rev. C **79**, 064904 (2009).
 - [4] J. Weiner, V. S. Bagnato, S. Zilio and P. S. Julienne, Rev. Mod. Phys. **71**, 1 (1999)
 - [5] S. Osnaghi, P. Bertet, A. Auffeves, P. Maioli, M. Brune, J. M. Raimond, and S. Haroche, Phys. Rev. Lett. **87**, 037902 (2001).
 - [6] L. Xu, W. W. Zhang, and S. R. Nagel, Phys. Rev. Lett. **94** 184505 (2005).
 - [7] M. M. Driscoll and S. R. Nagel, Phys. Rev. Lett. **107**, 154502 (2011).
 - [8] F. Savart, Ann. de Chim. **54**, 56 (1833).
 - [9] C. Clanet, J. Fluid Mech. **430**, 111 (2001).
 - [10] X. Cheng, G. Varas, D. Citron, H. M. Jaeger, and S. R. Nagel, Phys. Rev. Lett. **99** 188001 (2007).
 - [11] E. C. Rericha, C. Bizon, M. D. Shattuck, H. L. Swinney, Phys. Rev. Lett. **88** 014302 (2001).
 - [12] C. R. Wassgren, J. A. Cordova, R. Zenit, A. Karion, Physics of Fluids **15**, 3318 (2003).
 - [13] J. F. Boudet, J. Cassagne, and H. Kellay, Phys. Rev. Lett. **103**, 224501 (2009).
 - [14] J. S. Uehara, M. A. Ambroso, R. P. Ojha, and D. J. Durian, Phys. Rev. Lett. **90**, 194301 (2003).
 - [15] D. Lohse, R. Rauhé, R. Bergmann, and D. van der Meer, Nature (London) **432**, 689 (2004).
 - [16] H. Katsuragi, Phys. Rev. Lett. **104**, 218001 (2010).
 - [17] H. Siringhaus, *et al.*, Science **290**, 5499, 2123-2126, (2000).
 - [18] G. X. Chen, T. J. Kwee, K. P. Tan, Y. S. Choo and M. H. Hong, Appl. Phys. A **101**, 249 (2010).
 - [19] J. Ellowitz, N. Guttenberg and W. W. Zhang, arXiv:1201.5562 (2012).
 - [20] E. Azanza, F. Chevoir and P. Moucheron, J. Fluid Mech, **400**, 199 (1999).
 - [21] N. Guttenberg, arXiv:1203.6680 (2012).
 - [22] Y. J. Huang, C. K. Chan, and Piroz Zamankhan, Phys. Rev. E **82**, 031307 (2010).
 - [23] P. A. Cundall and O. D. L. Strack, Geotechnique, **29**, 47 (1979).
 - [24] S. Yuu, T. Abe, T. Saitoh and T. Umekage, Adv. Powder Technol. **6** 259 (1995).
 - [25] D. Goldman, M. D. Shattuck, C. Bizon, W. D. McCormick, J. B. Swift, and H. L. Swinney, Phys. Rev. E. **57**, 4831 (1998).
 - [26] L. Labous, A. D. Rosato and R. N. Dave, Phys. Rev. E. **56**, 5717 (1997).
 - [27] T. Sano and H. Hayakawa, in *Proceedings of ICTAM 23rd Int. Congress of theoretical and applied mechanics* (to be published).
 - [28] R. Goetz and R. Lipowsky, J. Chem. Phys. **108**, 7397 (1998).
 - [29] J. T. Jenkins and M. W. Richman, Phys. Fluids. **28**, 3485 (1985).
 - [30] V. Garzó and J. W. Dufty Phys. Rev. E **59** 5895 (1999).
 - [31] J. F. Lutsko, Phys. Rev. E **72** 021306 (2005).
 - [32] J. T. Jenkins and C. Zhang, Phys. Fluids **14** 1228 (2002).
 - [33] D. K. Yoon and J. T. Jenkins, Phys. Fluids **17** 083301 (2005).
 - [34] K. Saitoh and H. Hayakawa, Phys. Rev. E **75** 021302 (2007).
 - [35] S. Torquato, Phys. Rev. E **51**, 3170 (1995).
 - [36] A. Kawarada and H. Hayakawa, J. Phys. Soc. Jpn. **73**, (2004).
 - [37] O. R. Walton and R. L. Braun, J. Rheol. **30**, 949 (1986).
 - [38] M. Otsuki and H. Hayakawa, Phys. Rev. E. **83**, 051301(2011).